Phases and phase transitions in the mixed molecular system (NaCN)1x(KCN)x

T. Schräder, Alois Loidl, T. Vogt

Angaben zur Veröffentlichung / Publication details:

Schräder, T., Alois Loidl, and T. Vogt. 1990. "Phases and phase transitions in the mixed molecular system (NaCN)1x(KCN)x." Zeitschrift für Physik B Condensed Matter 79 (3): 423–30. https://doi.org/10.1007/bf01437653.

Phases and phase transitions in the mixed molecular system $(NaCN)_{1-x}(KCN)_x$

T. Schräder[1], A. Loidl[1], and T. Vogt[2]

[1] Institut für Physik, Universität Mainz, Federal Republic of Germany
[2] Institut Laue-Langevin, Grenoble, France

The phase diagram of $(NaCN)_{1-x}(KCN)_x$ was examined by neutron powder diffraction in the temperature range $5\,K \leqq T \leqq 300\,K$. Several non-cubic low-temperature phases were identified for concentrations $x < x_{c1} = 0.15$ and $x \geqq x_{c2} = 0.89$. Lattice parameters and ferroelastic deformations were determined from the observed powder patterns. The phase transformations were characterized following the temperature dependence of the appropriate order parameters.

I. Introduction

On cooling from room-temperature the ionic molecular crystals NaCN and KCN display two successive Landau-type phase transitions. At high temperatures and ambient pressure they exhibit a plastic phase of cubic symmetry ($Fm3m$). At T_c, both compounds transform via a ferrodistortive first-order transition into an intermediate body centered orthorhombic phase ($Immm$) [NaCN: $T_c = 288$ K, KCN: $T_c = 168$ K] [1]. The transition results from a strong coupling of the rotational degrees of freedom of the CN^- molecules to T_{2g} lattice strains [2]. The intermediate phase is characterized by long-range orientational order with the CN^- axis oriented along the (110) direction of the high-temperature cubic phase. On further cooling, at T_E the residual head to tail disorder of the CN^- dipoles is removed by a continuous order-disorder transition into an antiferroelectrically ordered ground state ($Pmnm$) [NaCN: $T_E = 172$ K, KCN: $T_E = 83$ K) [1]. The transition temperatures of T_c and T_E for KCN and NaCN were determined by thermodynamic measurements [3]. The structures of the low-temperature phases were studied by X-ray [4, 5] and neutron [6, 7] powder diffraction and have also been the subject of an intense theoretical work [8–11].

Solid solutions of alkali cyanides and alkali halides like $(KBr)_{1-x}(KCN)_x$ [12, 14], $(KCl)_{1-x}(KCN)_x$ [14–17] and $(NaCl)_{1-x}(KCN)_x$ [18] show fascinating $x-T$ phase diagrams. With increasing dilution of the cyanide ions by the spherical halide ions Br^- or Cl^- the transition temperatures decrease. Depending on concentration, the mixed systems transform into a variety of different non-cubic structures which can be understood as spontaneous deformations of the cubic parent phase. Below a threshold concentration x_c a low-temperature orientational glass state was identified [12, 13, 17, 18]. The relation of the appearance of polymorphism and the tendency to form an amorphous state is well known for the canonical glass SiO_2 [19] and was also studied for ice [20].

It has been proposed that for the mixed cyanide systems the coupling between the orientational degrees of freedom and internal random strain fields is an important mechanism for the glass formation process as well as for the polymorphic behaviour [16, 21, 22]. In this context mixed alkali cyanides have received attention, where only the alkali metal ions are randomly substituted. In $(RbCN)_{1-x}(KCN)_x$ and $(NaCN)_{1-x}(KCN)_x$ random strains are introduced by the implantation of cations of different size on the alkali sublattice. Due to a small difference in size of the substituents ($r_{Rb^+}/r_{K^+} = 1.11$), $(RbCN)_{1-x}(KCN)_x$ transforms into non-cubic ground states over the entire concentration range [23, 24]. However $(NaCN)_{1-x}(KCN)_x$ (with $r_{K^+}/r_{Na^+} = 1.36$) displays a low-temperature glass state of cubic symmetry in a wide range of composition [24]. Because the CN^- sublattice is preserved, this type of mixed system allows the study of the influence of random strains on the behaviour of the orientational degrees of freedom. In the present article we extend earlier structural information in $(NaCN)_{1-x}(KCN)_x$ to allow a closer insight into the polymorphic behaviour of this glass-forming system.

II. Experimental

Single crystals of $(NaCN)_{1-x}(KCN)_x$ with actual concentrations $x = 0.02, 0.04, 0.06, 0.08, 0.90, 0.95, 0.96$ and pure NaCN as a reference system were supplied by J. Albers from the Fachbereich Physik of the Universität des Saar-

landes. The crystals were grown from the melt using a conventional Czochralski technique. The actual concentrations systematically differ from the nominal composition of melt and were determined from the room-temperature lattice constants assuming Vegard's law [25].

The powder samples were prepared by grinding lumps of single crystals with mortar and pestle in a controlled argon gas atmosphere to avoid hydrolysation of the extremely hygroscopic material. In the same atmosphere the powder then was loaded into a vanadium can of 10 mm diameter which was sealed with an indium O-ring.

The neutron powder diffraction measurements were performed on the instrument *D 1B*, a two axis powder diffractometer with a curved multidetector system, located on a thermal neutron guide at the ILL Grenoble. A pyrolytic graphite (002) monochromator was used to select an incident wave length of $\lambda = 2.52$ Å. The range of scattering angle $\Delta 2\vartheta = 80$ deg is covered simultaneously by an ensemble of 400 detector elements which are calibrated with a vanadium standard. During all measurements the scattering angle 2ϑ ranges from 25° to 105°. The sample temperature was varied in the range 4 K to 300 K using a conventional liquid helium flow cryostat. A programmable temperature controller allowed a continuous variation of temperature with fixed cooling and heating rates.

III. Results and analysis

Figure 1 shows a tpyical result obtained from neutron powder thermo-diffractometry for $(NaCN)_{0.05}(KCN)_{0.95}$. Here neutron intensities are plotted as a function of the scattering angle at different temperatures. The powder spectra were recorded in roughly equidistant steps of temperature, increasing from 6 K (front) to 298 K (rear). At high temperatures the range in the scattering angle 2ϑ from 25° to 105° covers the cubic lines from (111) to (400). Contaminations of the spectra due to scattering of neutrons by the cryostat material are marked by small arrows. Since they do not exhibit a distinct temperature dependence they are easily identified and excluded from the data analysis.

For the mixed cyanides structural phase transitions could clearly be identified from the powder patterns by the appropriate splitting of the cubic lines. For ferroelastic transitions the development of satellites below T_c shows whether the transition is of continuous or discontinuous character. For all crystals investigated, transition temperatures were obtained from the occurrence of peak splittings or the appearance of (010) primitive reflections in the case of antiferroelectric order-disorder transition displayed by the powder patterns.

A. Phase diagram

A first schematic phase diagram of $(NaCN)_{1-x}(KCN)_x$ was examined by optical transmission experiments by Lüty and Ortiz-Lopez [24]. In contrast to alkali halide-alkali cyanide mixtures, $(NaCN)_{1-x}(KCN)_x$ displays an almost symmetric type of phase diagram and a low-T orientational glass state was proposed over a wide range of intermediate concentration $0.15 = x_{c1} \leqq x \leqq x_{c2} = 0.9$.

The existence of a cubic low-temperature glass state in $(NaCN)_{1-x}(KCN)_x$ was confirmed by previous dif-

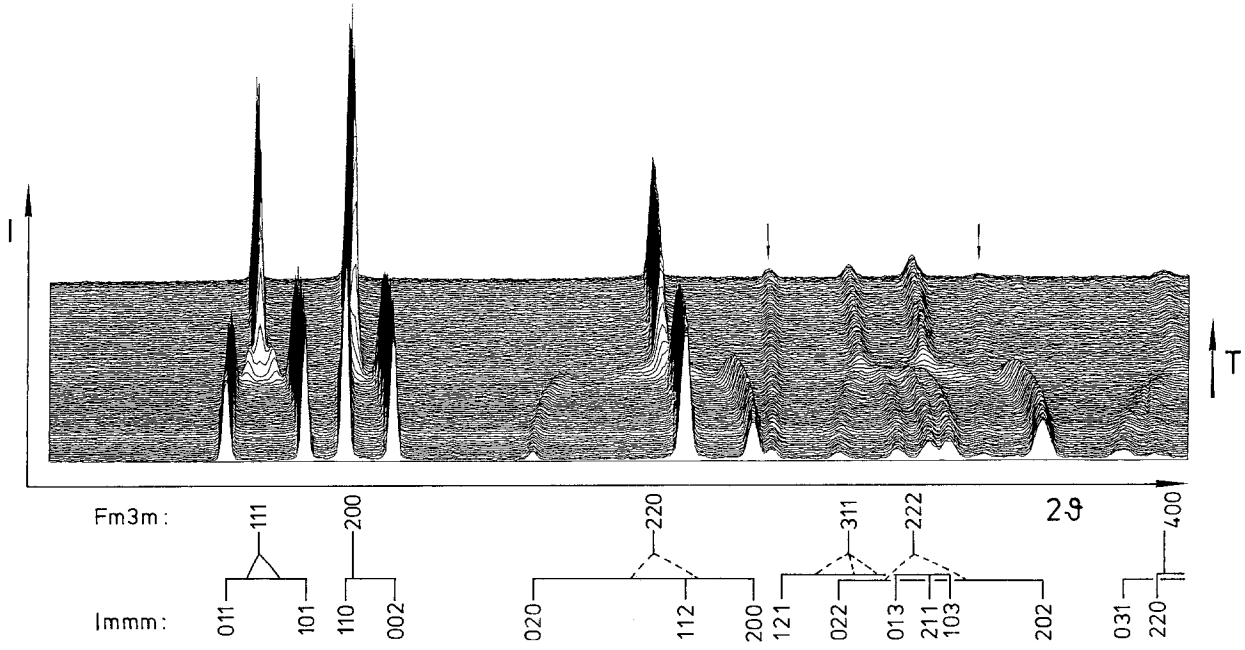

Fig. 1. Neutron powder patterns of $(NaCN)_{0.05}(KCN)_{0.95}$ as recorded by continuous variation of temperature. The scattering angle ranges from 25 deg to 104 deg and the temperature is increasing from 6 K (front) to 298 K (rear). Contamination of the spectra by reflections of the cryostat are indicated by arrows. Cubic and orthorhombic lines are labeled in the splitting scheme shown below

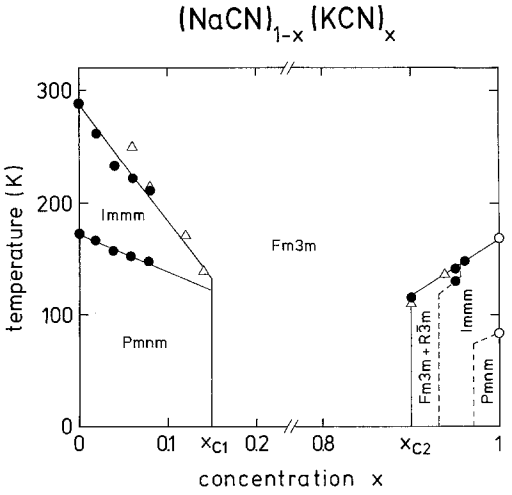

Fig. 2. Phase diagram of $(NaCN)_{1-x}(KCN)_x$. Transition temperatures, as determined in the present experiment (●), are plotted versus the actual concentration of KCN, randomly diluted in NaCN. Data for $x=1$ (○) were obtained from [3]. Data determined by optical transmission measurements (△) were obtained from [24]. Solid lines are drawn to guide to the eye. For $x>x_{c2}$ phase boundaries are drawn schematically by dashed lines

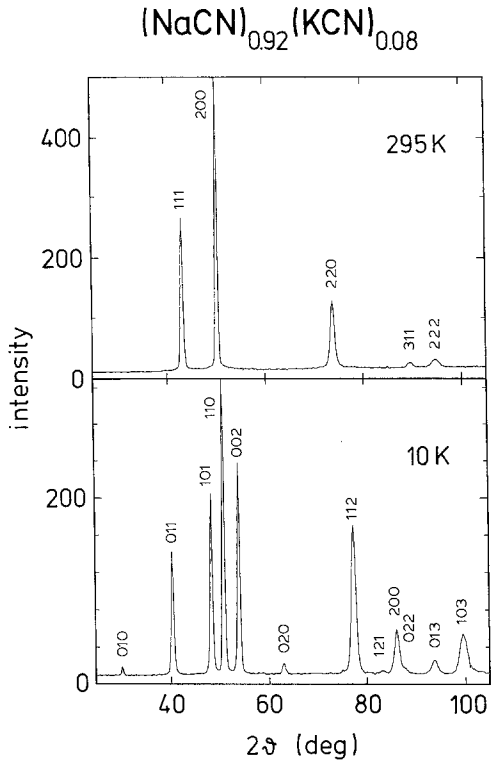

Fig. 3. Powder diffraction data of $(NaCN)_{0.92}(KCN)_{0.08}$ recorded at high and low temperature. The spectrum at 5 K displays the (010) primitive orthorhombic reflection at low scattering angle

fraction experiments [25, 26]. Structural information about the non-cubic phases existed only for $x=0.02$ and $x=0.95$ [25]. Orthorhombic low-temperature phases were identified with antiferroelectric order for $x=0.02$ ($Pmnm$) and residual dipolar disorder for $x=0.95$ ($Immm$).

In the present work both mixed crystals are reinvestigated by thermo-diffractometry. In addition, mixed crystals with concentrations $x=0.04$, 0.06, 0.08, 0.90, and 0.96 have been studied. With the exception of $x=0.90$, all low-temperature states exhibit a single phase. This allowed a clear identification of the non-cubic phases deduced from observed peak splittings. Principle schemes of peak splittings, resulting from homogeneous deformations of a fcc-parent phase, are listed by Gerwald et al. [27] together with appropriate symmetry information. For all mixed crystals investigated the transition temperatures and symmetry information obtained from the powder patterns are collected in the $x-T$ phase diagram of Fig. 2.

a. Sodium-rich compounds. The mixed crystals with concentration $x=0.02$, 0.04, 0.06 and 0.08 display the same subsequent phase transitions as observed in the pure cyanids NaCN and KCN. Indications of coexistences with other non-cubic phases were not detected. In particular, antiferroelectric (AFE) order is established for all concentrations $x<x_{c1}$. In Fig. 3 selected neutron powder spectra are shown for $x=0.08$ recorded at room temperature and 10 K. For the low-temperature orthorhombic phase only lines with $h+k+1=2n$ are indexed. The appearance of a (010) reflection indicates the onset of electric order in a primitive orthorhombic cell. Recent powder diffraction data in $x=0.11$, 0.13 and 0.16 revealed that the AFE-order even survives up to the critical concentration $x_{c1}=0.16$ [28]. Since only measurements at 5 K exist for these concentrations the data are excluded from the present analysis.

The ferroelastic transition temperatures T_c display an extremely strong linear decrease with increasing cationic disorder (see Fig. 2). This is in general agreement with results obtained from optical transmission experiments [24] which are also included in Fig. 2. Significant deviations are only apparent for $x=0.06$.

Also for the continuous order-disorder transition the transition temperatures T_E vary linearly with the concentration x. However, in contrast to $T_c(x)$ ($\Delta T_c/\Delta x \approx 10\,\mathrm{K}/\%\mathrm{K}^+$) the decrease of $T_E(x)$ ($\Delta T_E/\Delta x \approx 2.5\,\mathrm{K}/\%\mathrm{K}^+$) is more moderate.

b. Potassium-rich compounds. In the concentration range $x \geqq x_{c2}$ three mixed crystals with concentrations $x=0.90$, 0.95, 0.96 have been investigated. Transitions into several non-cubic low-T phases could be identified by the splitting of the fcc-lines. The transition temperatures T_c were found to be in good agreement with the results of [24]. Again the substitution of K^+ ions by the smaller Na^+ ions results in an almost linear decrease of T_c with the concentration x. However, the slope $\Delta T_c/\Delta x \approx 5\,\mathrm{K}/\%\mathrm{K}^+$ is much smaller than observed for Na^+ rich mixed crystals.

$(NaCN)_{0.04}(KCN)_{0.96}$ discontinuously transforms to a single phase ferroelastic order ($Immm$) at $T_c=148$ K. Additional primitive reflections are absent down to the lowest temperatures which is indicative for an electrically disordered ground state. In contrast to Na^+-rich mixed

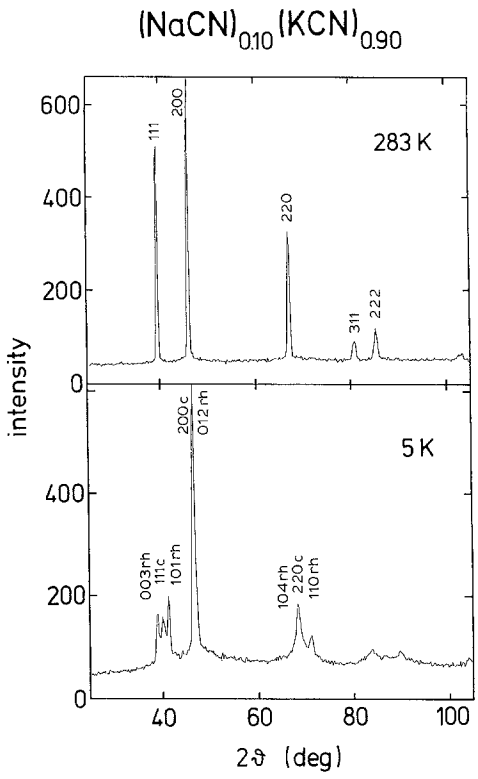

Fig. 4. Powder diffraction data of $(NaCN)_{0.10}(KCN)_{0.90}$ recorded at high and low temperature. The spectrum at 5 K displays a coexistence of cubic and rhombohedral lines. The indices h, k, l of the rhombohedral lines are given in a hexagonal setting for $R\bar{3}m$, assuming a stretched cubic cell

crystals, where dipolar order was found up to $x_{c1}=0.16$ [28] the electric order is suppressed already by 4% Na^+ impurity ions disolved in KCN. This asymmetry cannot be understood in terms of a simple random field model.

On cooling from room-temperature, the mixed crystal with $x=0.95$ displays a splitting of the cubic lines at $T=140$ K. On further cooling ferroelastic order ($Immm$) is established at $T=130$ K. Dipolar order could not be identified down to 4 K (see Fig. 1). In the intermediate phase the splitting could only be clearly resolved near the previous cubic (111) reflection which displays two satellites as demonstrated by the powder pattern of Fig. 1. Since the (200) Bragg reflection reveals no splitting, we assume that the intermediate phase is rhombohedral ($R\bar{3}m$). The intensity distribution among the two rhombohedral satellites (101) and (003) of the previous cubic (111) is unclear so that we could not determine whether the cell is squeezed or stretched. While the rhombohedral lines continuously develop from the cubic reflections, the onset of the orthorhombic lines is definitely discontinuous.

$(NaCN)_{0.10}(KCN)_{0.90}$ is close to the critical concentration x_{c2} and develops a continuous line-splitting near 108 K. The splitting scheme favours a coexistence of a cubic and rhombohedral phase which persists down to the lowest temperatures. Selected powder profiles recorded for $x=0.90$ at 283 K and 5 K are displayed in Fig. 4. At 5 K the ratio of both components is roughly determined from peak intensities as 37% cubic and 63% rhombohedral. For a rhombohedral distortion an intensity ratio of 3:1 is required for the two satellites of the cubic (111) reflection. A cubic cell squeezed along one of the body diagonals gives rise to an intensity ratio 3:1 with the stronger peak appearing at lower scattering angles. This type of distortion was observed in $(KBr)_{0.35}(KCN)_{0.65}$ [13]. For a cubic cell stretched along a body diagonal the intensity ratio of the line-splitting is exactly reversed. This is the case for the rhombohedral phase of CsCN [29] where the CN^- molecules are ferroelastically ordered along one (111) direction. The low-temperature spectrum of $x=0.90$ reveals the stronger peak at higher scattering angles. However, the intensities do not show the correct ratio expected for a stretched cubic cell. The cubic as well as the rhombohedral lines attain wings of strong diffuse scattering which increase for higher scattering angles. In addition the profile is characterized by a large static Debye-Waller factor. Both findings are typical fingerprints of the orientational glass state in mixed cyanides and are known to result from frozen-in shear distortions [13, 30].

Near the critical concentrations, $(NaCl)_{1-x}(KCN)_x$ [18] and $(KBr)_{1-x}(KCN)_x$ [13, 30] exhibit a rhombohedral phase at low-T, too. Knorr et al. [30] demonstrated that for $(KBr)_{0.35}(KCN)_{0.65}$ the rhombohedral ground state could be suppressed on thermal cycling. The authors explained their findings in terms of domain wall formation and interpreted the orientational glass state in $(KBr)_{1-x}(KCN)_x$ as a consequence of polymorphism. Because of these experimental results we applied cycle procedures to $(NaCN)_{0.10}(KCN)_{0.90}$ in order to test if the rhombohedral phase could be suppressed by sample history effects. The powder sample was cycled 5 times through the transition with annealing temperatures not higher than 40 K above T_c. In contrast to the results of [30] no effects of the thermal treatment on the structural behaviour of $x=0.90$ could be observed. T_c was reproduced within the estimated deviations. On repeated cooling the sample displayed the structural transition from $Fm\bar{3}m$ into a coexistence of cubic and rhombohedral ($R\bar{3}m$) phases without exception. In particular the intensity ratio of the cubic and rhombohedral lines remains unchanged during the cycling procedure.

The powder diffraction data were quantitatively analyzed using the refinement procedures given by Pawley [31]. For a given structure, peak positions and intensities were fitted to the measured powder profiles. The machine parameters U, V, W and the zero point of the 2ϑ scale were also included. From these fits we obtained the temperature dependent lattice parameters of the cubic and orthorhombic phases.

Results for the temperature dependence of the cell volume are shown in Fig. 5. For $x<x_{c1}$ the first-order phase transition is represented by a discontinuous reduction of the crystal volume of approximately 1.3%. The onset of antiferroelectric order gives rise to weak anomalies in $V(T)$ at lower temperatures as indicated by arrows. A considerably smaller step in the cell volume (0.2%) was observed for $x=0.96$. The step in $V(T)$ nearly vanishes for $x=0.95$, although the transition from $R\bar{3}m$ to $Immm$ definitely is of first order. We conclude that

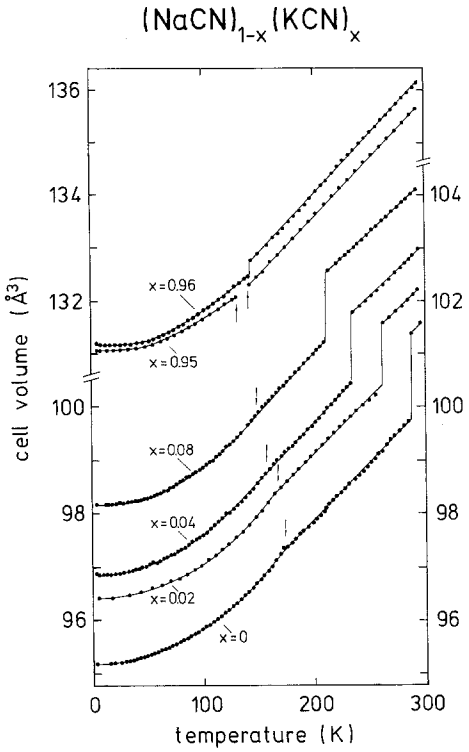

Fig. 5. Temperature dependence of the orthorhombic cell volume determined for different concentrations $x<x_{c1}$ and $x\geqq x_{c2}$. For better comparison the volume of the cubic phases is reduced by a factor of 2. Solid lines are drawn to guide the eye

the structural transitions in $(NaCN)_{1-x}(KCN)_x$ are strongly of first order on the Na-rich side of the phase diagram and that they become almost of second order on the K-rich side, close to the critical concentration.

B. Order parameter

a. Ferroelastic transition: $Fm3m-Immm$. The first-order transition from the high-temperature cubic phase ($Fm3m$) into the orthorhombic phase ($Immm$) is accompanied by lattice strains of A_{1g}, T_{2g} and E_g symmetry. The strains are represented by a volume change, a uniform shear distortion and a uniaxial compression perpendicular to the shear plane. The cell parameters and the elements e_{ij} of the ferroelastic deformation tensor are given in Table 1 for room-temperature, the transition temperatures T_c and T_E and for the lowest temperatures.

Orthorhombic phases ($Immm$) were observed for $x=0$, 0.02, 0.04, 0.06, 0.08, 0.95 and 0.96. From the cell parameters a and b we calculated the shear angle with respect to the previous cubic cell. The temperature dependence of the shear angle $\Delta\gamma$ displays the behaviour of the primary order parameter and is plotted in Fig. 6 for six different concentrations. For Na^+-rich mixed crystals with concentrations $x<x_{c1}$ the order parameter displays a discontinuous jump of comparable magnitude at T_c, up to approximately 12.5°. Below T_c the shear angle then develops continuously reaching 16.2° for $x=0$ and 15.2° for $x=0.08$. The low-temperature values for $x=0.02$ and 0.04 scale with the concentration x. This can be understood by simple geometry. When the lattice dimensions are small, $\langle 110\rangle_c$ oriented CN^- molecules yield higher shear angles than in the case of larger lattice dimensions. The discontinuity at T_c is considerably smaller for K^+-rich mixed crystals and yields only about 9.2° deg for both mixed crystals with $x=0.95$ and $x=0.96$. At the lowest temperatures the shear angle reaches 11.68° for $x=0.95$ and 12.06° for $x=0.96$.

The shear distortion at the first-order transition from $Fm3m$ to $Immm$ is accompanied by an uniaxial compression (E_g). The order parameter in E_g symmetry is the relative change in the lattice constant c given by $\delta c=1-c_0/c_c$ where c_c denotes the lattice parameter in the cubic and c_0 in the orthorhombic phase. Fig. 7 displays the lattice constant c for $Fm3m$ and $Immm$ as determined from the fits following [31] for six different concentrations. In the high-temperature phase $c(T)$ ex-

Table 1. Cell parameters a, b, and c and the elements e_{ij} of the ferroelastic deformation tensor $\mathbf{T}_{ij}$ are given for room temperature, the transition temperatures (T_c) (*) and T_E (**) and for the lowest temperatures. For the $Immm$ and $Pmnm$ phases the cell parameters are described within a regular orthorhombic setting. For $x=0.90$ parameters of the rhombohedral phase ($e_{ii}=$const, $e_{ij}=$const for all $i\neq j$ and $e_{ii}\neq e_{ij}$) are given under the assumption of a stretched cubic parent phase

conc x	T(K)	Space group	a (Å)	b (Å)	c (Å)	e_{xx}	e_{xy}	e_{zz}
0	295	$Fm3m$	5.878	–	–	–	–	–
	288*	$Immm$	3.776	4.700	5.633	0.0202	0.1110	−0.0412
	172**	$Immm$	3.675	4.784	5.537	0.0182	0.1335	−0.0575
	5	$Pmnm$	3.621	4.823	5.446	0.0163	0.1446	−0.0730
0.02	295	$Fm3m$	5.892	–	–	–	–	–
	261*	$Immm$	3.781	4.709	5.646	0.0208	0.1115	−0.0400
	164**	$Immm$	3.699	4.779	5.568	0.0193	0.1300	−0.0532
	5	$Pmnm$	3.647	4.824	5.482	0.0184	0.1415	−0.0678
0.04	295	$Fm3m$	5.90	–	–	–	–	–
	233*	$Immm$	3.783	4.692	5.657	0.0183	0.1093	−0.0387
	156**	$Immm$	3.713	4.759	5.587	0.0179	0.1257	−0.0506
	10	$Pmnm$	3.658	4.814	5.502	0.0179	0.1389	−0.0651
0.06	295	$Fm3m$	5.920	–	–	–	–	–
	226*	$Immm$	3.800	4.718	5.655	0.0209	0.1100	−0.0415
	156**	$Immm$	3.714	4.775	5.590	0.0174	0.1272	−0.0525
	5	$Pmnm$	3.661	4.825	5.508	0.0170	0.1395	−0.0664
0.08	295	$Fm3m$	5.929	–	–	–	–	–
	211*	$Immm$	3.801	4.717	5.673	0.0205	0.1908	−0.0388
	148**	$Immm$	3.736	4.759	5.615	0.0178	0.1225	−0.0486
	10	$Pmnm$	3.683	4.815	5.536	0.0181	0.1357	−0.0620
0.90	295	$Fm3m$	6.445	–	–	–	–	–
	108*	$Fm3m$	6.374	–	–	–	–	–
	5	$R\bar{3}m$	4.588	–	–	0.0068	0.0112	0.0068
0.95	295	$Fm3m$	6.472	–	–	–	–	–
	130*	$Immm$	4.264	5.019	6.177	0.0231	0.0829	−0.0373
	5	$Immm$	4.190	5.145	6.084	0.0288	0.1052	−0.0517
0.96	295	$Fm3m$	6.482	–	–	–	–	–
	149*	$Immm$	4.268	5.020	6.185	0.0221	0.0820	−0.0375
	5	$Immm$	4.181	5.169	6.073	0.0288	0.1087	−0.0549

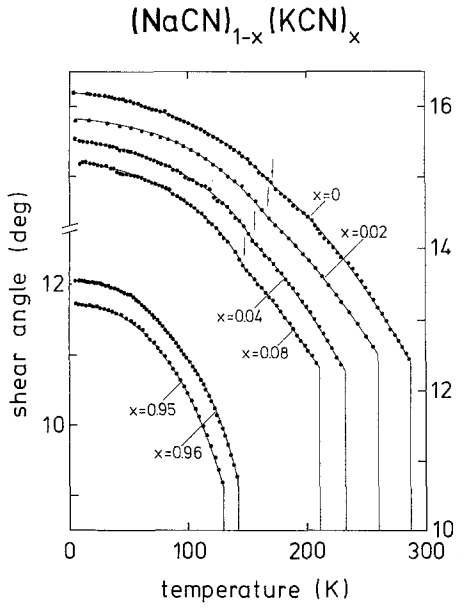

Fig. 6. Temperature dependence of the spontaneous shear strains below the cubic to orthorhombic phase transformation determined for concentrations $x<x_{c1}$ and $x\geqq x_{c2}$. For $x<x_{c1}$ anomalies due to the subsequent order-disorder transition are indicated by arrows. Solid lines are drawn to guide the eye

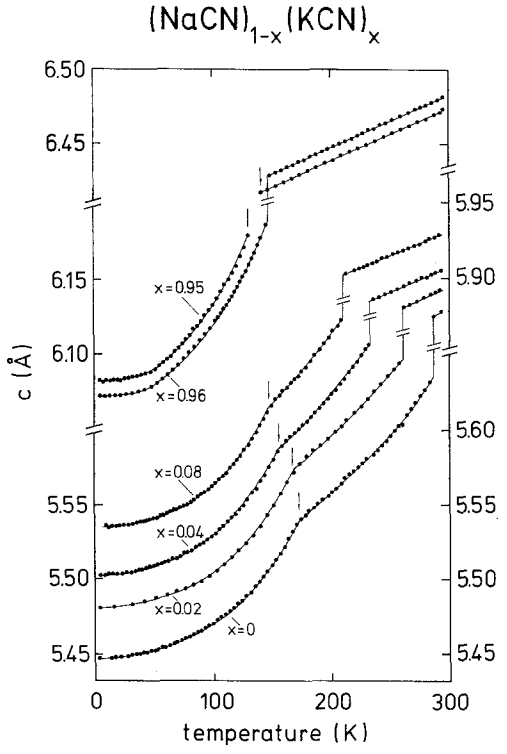

Fig. 7. Temperature dependence of the lattice parameter c determined both in the cubic high-T phases and in the orthorhombic low-T phases for different concentrations $x<x_{c1}$ and $x\geqq x_{c2}$. For $x<x_{c1}$ anomalies corresponding to the antiferroelectric order-disorder transition are indicated by arrows. For $x=0.95$ transition temperatures of the intermediate rhombohedral phase are also marked by arrows. Solid lines are drawn to guide the eye

hibits the expected linear behaviour in T. At T_c the c-axis drops by a comparable amount of 4%, independent on concentration. Below T_c in the orthorhombic phase the lattice constant c varies non-linearly with temperature demonstrating that $c(T)$ is dominated by the order parameter behaviour in E_g symmetry.

Furthermore, for concentrations $x=0$, 0.02, 0.04, 0.06 and 0.08 $c(T)$ shows remarkable anomalies at temperatures T_E where antiferroelectric ordering processes set in. In Fig. 7 these characteristic temperatures are marked by arrows. In the $Immm$ phase 180° reorientations of the CN^- molecules are still allowed but will be reduced when electrical order occurs. This may cause a further increase of the uniaxial compression below T_E.

b. Ferroelastic transition: $Fm3m-R\bar{3}m$. The cubic ($Fm3m$) to rhombohedral ($R\bar{3}m$) transition is realized either by stretching or squeezing the cubic cell along one of the four body diagonals. The ferroelastic deformation tensor $\mathbf{T}_{ij}$ [32] is defined by $e_{ij}=\sin(\Delta\alpha')/\sqrt{2}\, a_c'/a_c$ for all $i\neq j$ and $e_{ij}=(\cos(\Delta\alpha')\, a_c'/a_c)-1$ for $i=j$; $\Delta\alpha'$ denotes the shear angle measured between the axis of the distorted and undistorted cubic cell. Indications of rhombohedral lines were observed for $x=0.90$ at low temperatures and for $x=0.95$ for a narrow regime of intermediate temperatures. A quantitative analysis of the present data is impossible for $x=0.95$. For $x=0.90$ the temperature dependence of the ferroelastic order parameter can hardly be determined. According to the intensity ratio of the (101) and (003) Bragg reflections the type of rhombohedral distortion remains unclear. We analysed the data for $x=0.90$ on the assumption of a stretched cubic parent phase. The deviations $\Delta\alpha$ from the cubic rectangles represent the primary order parameter of the transition. $\Delta\alpha$ continuously develops at T_c and reaches 1.3° at the lowest temperatures. The elements of the ferroelastic deformation tensor T_{ij}, determined at $T=5$ K are given in Table 1.

c. Antiferroelectric transition: $Immm-Pmnm$. As mentioned above indications of further transitions were observed for $x<x_{c1}$ as anomalies in the temperature dependence of the lattice constants. The anomalies are marked by arrows in Figs. 5, 6, 7 and were found to be much more pronounced for $c(T)$ than in the temperature dependence of the cell volume $V(T)$ and the shear angle $\Delta\gamma(T)$. Indications for the continuous antiferroelectric phase transition were also observed in the temperature dependence of the elastic properties in pure KCN [33] and in the mixed cyanides [34]. Due to the dipolar order-disorder transition contributions of higher order terms to the ferrodistortive order parameter are possible.

A definite proof of the antiferroelectric order-disorder transition is the appearance of the primitive orthorhombic reflections in the low-temperature powder profiles. In particular the (010) reflection is well resolved at low scattering angles [6, 7, 25] (see e.g. Fig. 3). Its intensity is related to the order parameter η which describes the disappearance of symmetry elements due to the antiferroelectric transition. It has been shown by the-

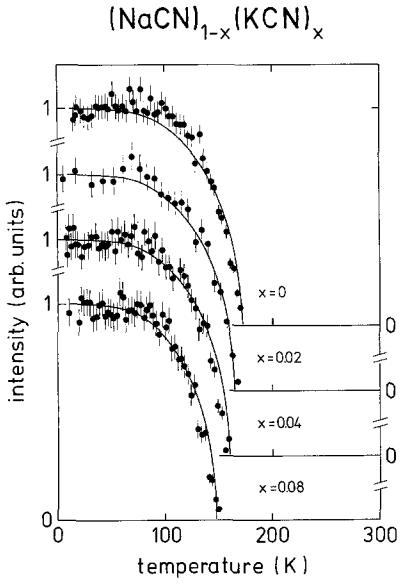

Fig. 8. Intensity of the (010) primitive orthorhombic reflection versus the temperature, observed for concentrations $x=0$, 0.02, 0.04, 0.08. The order parameter behaviour of a spin $^1/_2$ Ising system is calculated in a mean field approximation and demonstrated by solid lines

oretical studies that additional dipolar moments, induced either by lattice vibrations [9] or by static displacements [10] are essential for the formation of an AFE ground state. In the cyanides the existence of static cationic displacements was confirmed by experimental work [25]. However, due to the limited resolution of the powder diffractometer used in the measurements of the present data, a refinement of atomic positions was not realistic.

Here we only want to concentrate on the order parameter behaviour of the AFE phase transition. The dipolar ordered ground state of KCN and NaCN was theoretically studied in detail [8, 35, 36]. Stokes [36] presented a simple model for CN^- reorientations in the low-T ground state of KCN and NaCN, based on a change in activation energy for the two possible orientations when the systems transform from $Immm$ to $Pmnm$. He illustrated his results by Monte Carlo computer simulations and calculated the order parameter using an Ising model. From Raman allowed modes, observed for $T<T_E$, Dultz [35] derived critical effects at the electrical order-disorder transition in KCN. The order parameter, represented by the intensity I of the Raman allowed lines was fitted using $\eta^2 \sim I=(T_c-T)^\beta$, with a critical exponent $\beta=0.66$. Within a mean field approximation dos Santos et al. [8] derived the order parameter of the electric transition in KCN, starting from a simple microscopic Hamiltonian based on electric dipole-dipole interactions between the CN^- molecules. However, the AFE configuration proposed by his model is in contradiction to neutron scattering results [6, 7, 25].

The temperature dependence of the (010) reflection is displayed in Fig. 8 for concentrations $x=0$, 0.02, 0.04, 0.08. The order parameter of the continuous phase transition can be described analogous to the spontaneous magnetisation in magnets by a spin $^1/_2$ Ising system [13]. In Fig. 8 a spin $^1/_2$ Brillouin function is fitted to the experimentally observed intensity of the (010) reflection. The data and fits are in reasonable agreement.

IV. Conclusions

The phase diagram of $(NaCN)_{1-x}(KCN)_x$ has been investigated in detail. Specifically the nature of the phase transitions was studied following the temperature dependence of the primary order parameters. The dilution of either KCN by smaller Na^+ cations or NaCN by larger K^+ cations leads to a completely different structural behaviour of the mixed crystals:

Na-rich mixed crystals exhibit a sequence of elastic and electric phase transitions analogous to those found in the pure cyanides NaCN and KCN: they display ferroelastic transitions from $Fm3m$ to $Immm$ (see also [28]). The primary order parameter is defined by the shear angle $\Delta\alpha$ which describes the distortion of the high-temperature cubic parent phase. The transitions were found to be strongly of first-order. All mixed crystals with $x<x_{c1}$ show primitive reflections which evolve continuously for $T<T_E$. This reveals transitions into a antiferroelectrically ordered ground state. The intensity of the primitive (010) reflection is related to the order parameter of the continuous order-disorder transition and can roughly be described by a spin $^1/_2$ Brillouin function. At T_E the temperature dependence of the lattice parameters displays distinct anomalies, indicating that the antiferroelectric ordering process is also coupled to lattice deformations.

K-rich mixed crystals display structural phase transitions up to the critical concentration $x_{c2}=0.9$. Mixed crystals with $x=0.96$ and $x=0.95$ are orthorhombic at low temperatures. The 95% crystal displays rhombohedral lines for a small intermediate temperature range. For concentrations $0.9<x<0.93$ we suggest that probably either rhombohedral and orthorhombic or rhombohedral and cubic phases are coexistent at low-T. A crystal with $x=0.9$, which is coincident with the critical concentration x_{c2}, transforms only partially into a rhombohedral structure. This transition is close to second order. The ratio of the cubic and rhombohedral components as well as T_c are unaffected by thermal cycling.

Despite the orthorhombic structure ($Immm$), observed for $x=0.95$ and $x=0.96$, no indications of electric order were found. Already a small cationic disorder of 4% Na^+ ions, randomly diluted in KCN, suppresses the antiferroelectric order. For KCN the increase of reorientational barriers due to Na^+ doping seems to be much more effective than K^+ doping for pure NaCN: the transition temperature is much lower for KCN ($T_E=83$) than for NaCN ($T_E=172$ K). Thus, a further increase of the hindering barriers and a decrease of the dipole-dipole interactions push the dipolar relaxation times towards long times at the hypothetic ordering temperature and electric order cannot be established for $x=0.95$ and 0.96 within the experimental time scale.

This work has been funded by the German Federal Minister for Research and Technology (Bundesminister für Forschung und Technologie (BMFT) under contract No. 03-L01MAI-0(C1-56)) and by the Sonderforschungsbereich SFB 262 (Mainz).

References

1. Lüty, F.: Defects in insulating crystals. Turkevitch, V.M., Swartz, K.K. (eds.), pp. 69–89. Berlin, Heidelberg, New York: Springer 1981
2. Michel, K.H., Naudts, J.: J. Chem. Phys. **68**, 216 (1977)
3. Suga, H., Matsuo, T., Seki, S.: Bull. Chem. Soc. Jpn. **38**, 1115 (1965) Matsuo, T., Suga, H., Seki, W.: Bull. Chem. Soc. Jpn. **41**, 583 (1968)
4. Verwell, H.J., Bijvoet, J.M.: Z. Krist. **100**, 201 (1938)
5. Bijvoet, J.M., Lely, J.A.: Rec. Trav. Chim. Pays-Bas **59**, 908 (1940)
6. Fontaine, D.: C. R. Acad. Sc. Paris **281**, 443 (1975)
7. Rowe, J.M., Rush, J.J., Prince, E.: J. Chem. Phys. **66**, 5147 (1977)
8. Santos, R.R. dos, Koiller, B., Weid, J.P. von der, Costa Ribeiro, S., Chaves, A.S., Sà Barreto, F.C.: J. Phys. C **11**, 4557 (1978)
9. Pirc, R., Vilfan, I.: Solid State Commun. **39**, 181 (1981)
10. Koiller, B., Davidovich, M.A., Scavarda do Carmo, L.C., Lüty, F.: Phys. Rev. B **29**, 3586 (1984)
11. Ohno, E.: J. Phys. Soc. Jpn. **57**, 4265 (1988)
12. Knorr, K., Loidl, A.: Phys. Rev. B **31**, 5387 (1985)
13. Loidl, A., Schräder, T., Knorr, K., Böhmer, R., Mertz, B., McIntyre, G.J., Vogt, T., Mutka, H., Müllner, M., Jex, H., Haussühl, S.: Z. Phys. B – Condensed Matter **75**, 81 (1989)
14. Rowe, J.M., Bouillot, J., Rush, J.J., Lüty, F.: Physica B **136**, 498 (1986)
15. Bourson, P.G., Gorczyca, G., Durand, D.: Cryst. Latt. Def. Amorph. Mater **16**, 311 (1987)
16. Civera Garcia, E., Knorr, K., Loidl, A.: Phys. Rev. B **36**, 8517 (1987)
17. Bouillot, J., Soubeyroux, J.L., Lüty, F.: Physica B **156** & **157**, 81 (1989)
18. Elschner, S., Knorr, K., Loidl, A.: Z. Phys. B – Condensed Matter **60**, 209 (1985)
19. Jäckle, J.: Rep. Prog. Phys. **49**, 171 (1986)
20. Behnke, G., Biltz, H., Büttner, H.: Phys. Rev. Lett. **56**, 1276 (1986)
21. Michel, K.H.: Z. Phys. B – Condensed Matter **68**, 259 (1987)
22. Lewis, L., Klein, M.L.: Phys. Rev. Lett. **57**, 2698 (1986) Lewis, L., Klein, M.L.: J. Phys. Chem. **91**, 4990 (1987)
23. Fossum, J.O., Garland, C.W., Wells, A.: Preprint (1987)
24. Ortiz Lopez, J.: Ph. D. Thesis, University of Utah, 1983; Lüty, F., Ortiz Lopez, J.: Phys. Rev. Lett. **50**, 1289 (1983)
25. Schräder, T., Loidl, A., Vogt, T.: Phys. Rev. B **39**, 6186 (1989)
26. Loidl, A., Schräder, T., Böhmer, R., Knorr, K., Kjems, J.K., Born, R.: Phys. Rev. B **34**, 1238 (1986)
27. Gerward, L., Staun Olsen, J., Benedict, U.: Physica B **144**, 72 (1986)
28. Schräder, T., Loidl, A., Vogt, T.: Ferroelectrics (in press)
29. Knopp, G., Knorr, K., Loidl, A., Haussühl, S.: Z. Phys. B – Condenset Matter **51**, 259 (1983)
30. Knorr, K., Civera Garcia, E., Loidl, A.: Phys. Rev. B **35**, 4998 (1987)
31. Pawley, G.S.: J. Appl. Crystallogr. **14**, 357 (1981)
32. Aizu, K.: J. Phys. Soc. **28**, 706 (1970)
33. Rehwald, W., Sandercock, J.R., Rossinelli, M.: Phys. Status Solidi A **42**, 699 (1977)
34. Hessinger, J., Knorr, K.: Phys. Rev. Lett. **63**, 2749 (1989)
35. Dultz, W.: J. Chem. Phys. **65**, 2812 (1976)
36. Stokes, H.T., Swinney, R.D.: Phys. Rev. B **31**, 7133 (1985)

T. Schräder, A. Loidl
Institut für Physik der Universität
Staudinger Weg 7
D-6500 Mainz
Federal Republic of Germany

T. Vogt
Institut Laue-Langevin
F-38042 Grenoble
France